JOURNAL OF Applied Polymer SCIENCE

Preparation and Colorimetric Characterization of Polymeric Nanophotonic Structures

Mohammad Reza Shamshiri,[1] Ali Akbar Yousefi,[2] Farhad Ameri[1]

[1]Department of Color Physics, Institute for Color Science and Technology, 16765-654 Tehran, Iran

[2]Department of Plastic Engineering, Iran Polymer and Petrochemical Institute, 14965/115 Tehran, Iran

Correspondence to: A. A. Yousefi (E-mail: a.yousefi@ippi.ac.ir)

ABSTRACT: A spin-casting machine was designed and fabricated for preparation of multilayer polymer films from parent polymer solutions together with a polymeric dispersion of nanoparticles. The dispersion consists of polystyrene (PS)-based core coated with a poly(methyl methacrylate-*co*-butyl acrylate) shell. Multilayer structure of such films was confirmed using a scanning electron microscope A sandwiched dispersed nanoparticles cast from the spin-casting machine assumed a near to hexagonal arrangement. This structure affected the optical properties of the cast films. The films were characterized using colorimetric methods such as spectrophotometric and goniospectrophotometric techniques. Moreover, a dispersion of styrene-based nanoparticles is sandwiched between PS and poly(methyl methacrylate) layers. The multilayer sandwiched films illustrated a greenish color shift attributed to the formation of hexagonal structures. The dispersion of styrene-based nanoparticles within this sandwich restricts the observation of some wavelengths, which could be attributed to changes in the refractive indices of such samples. © 2012 Wiley Periodicals, Inc. J. Appl. Polym. Sci. 000: 000–000, 2012

KEYWORDS: optical properties; nanostructured polymers; spectroscopy

Received 24 June 2012; accepted 4 July 2012; published online
DOI: 10.1002/app.38313

INTRODUCTION

Photonic crystals (PC) are the structures that their refractive index periodically changes in space leads to a coherent scattering of light and alters the modes of propagation of light.[1] Recently, many different application are developed for these materials, such as data communication, nonlinear optics, industry, and medical applications.[2] The periodicity of spatial modulation in the refractive index of these materials can be in one, two, or three dimensions.[3–4] Due to their structures, light is reflected in a certain direction. The reflection intensity depends on parameters such as periodicity of PC and its refractive index contrast. Some frequencies are strongly reflected without almost any transmission.[5–7]

In a three-dimensional polymeric PC (PPC), the wavelength of reflected light, λ, is related to the spacing voids, d, via an approximation of Bragg-Snell's law as:[1]

$$k\lambda = 2d(n_{\text{eff}}^2 - \sin^2\theta)^{0.5} \quad (1)$$

where k is an integer, n_{eff} is the effective refractive index of the PPC, and θ is the angle of incidence of light with respect to the normal of the PPC.[1] For example, if spheres are arranged in a hexagonal arrangement with each sphere touching each other, the relationship between the sphere radius and the spacing of the voids will be $d = 1.633$ r.[8–18]

However, common three-dimensional PC have a high value of refractive index difference (Δn) between their component phases that leads to a full photonic bandgap, but Δn of the PPCs is intrinsically low due to relatively low refractive index of polymers which causes these materials do not have a full bandgap.[1] Nevertheless, the PPCs exhibit some special optical properties like wave guiding which are characteristic of full photonic bandgap materials.[19]

The color of the PPCs is dependent on the angle of viewing and ranges from red to violet. However, due to total internal reflection at a certain viewing angle, some wavelengths of light cannot leave the PPC. This angle is called critical angle (θ_C). For instance, if red is observed vertically, the yellow-green light leaves the PPC parallel to the surface. All shorter wavelengths cannot leave the PPC. According to Snell's law[8], the light's path and critical angle could be manipulated by changing the refractive index of the medium by which the PPC is surrounded. The PPCs are usually fabricated via melt compression,[9–12] vertical crystallization,[15] layer-by-layer processes,[14] emulsion polymerization,[20]

Applied Polymer SCIENCE

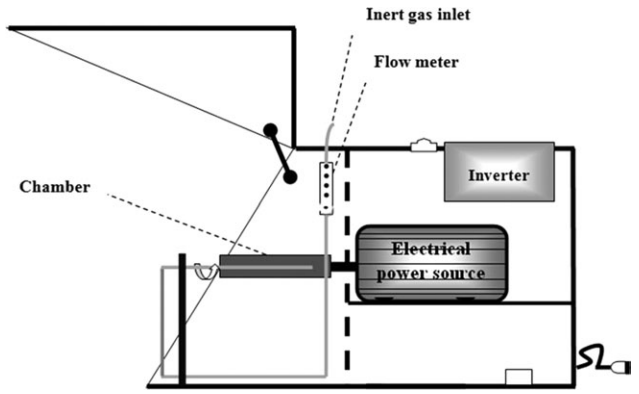

Figure 1. The schematic version of the spin-casting machine.

rotational shearing,[21] etc. These procedures are used to produce materials such as artificial opals,[9–12] pigments,[17] waveguides,[22] etc.[23]

An interference filter is an optical filter that reflects a portion of the spectral band and transmits others. Usually, these filters consist of multiple thin layers of dielectric material having different refractive indices.[24] Some optical filters are normally designed for normal incidence. However, any change in the incidence angle of the incoming light affects the transmitted wavelength of the filter, resulting in partial tunability.

In this article, design and assembling a spin-casting machine have been presented. The effect of centrifugal force on rearrangement of styrene-based nanoparticles was also investigated. The dispersion of styrene-based nanoparticles was sandwiched between multiple polystyrene (PS) and poly(methyl methacrylate) (PMMA) layers to produce a multilayer structure. Finally, the optical properties of multilayer structures were investigated via spectrophotometric and goniospectrophotometric techniques. The novelty of the work remains in the method of preparation of such nanostructured polymeric optical filters.

EXPERIMENTAL

Material

PS-1540 (Tabriz Petrochemical company, Tabriz, Iran) and PMMA-Plexiglas HFI-10-101 (Arkema company, Gunzburg, Germany) pair was used to prepare the polymeric multilayer films. The refractive indices of PS and PMMA are 1.59 and 1.49, respectively. Acetone, cyclohexane, and carbon tetrachloride solvents all from Merck company (Germany) were used. The method of preparation of the dispersion is reported elsewhere.[12,25] Such dispersion has a core-shell structure,[26] which was prepared via stepwise emulsion polymerization. The dispersion was composed of crosslinked PS-based nanoparticles chemically bonded to a poly(methyl methacrylate-*co*-butyl acrylate) shell. In addition, this dispersion is monodisperse in particle size distribution and its average particle size is about 160 nm. The refractive index of a dried film of the dispersion is 1.56.[25]

Description of the Spin-Casting Machine

This machine is made up of a cylindrical chamber connected to an electrical power source in which RPM and time can be controlled via an inverter. Through continuous injection of suitable amounts of polymeric solutions into the chamber and depositing layers via solvent evaporation method on its inner surface, ductile preforms could be prepared. A Teflon™ chamber was used to easily separate the preform from the chamber. Considering vulnerability of some polymeric solutions to humidity, an inert gas was purged into the chamber at a rate of 0.1 mL/min.[27–29] Fabrication of this spin-casting machine has several advantages amongst which economical aspects and flexibility in design are referable. A schematic version of the machine is depicted in Figure 1.

Table I. The Prepared Samples and Their Specification

Sample	Description
S1	One dispersion layer prepared using the film applicator
S2	One dispersion layer on the supportive layer
S3	Three-layer PS/dispersion/PMMA film on the supportive layer

Sample Preparation

Acetone and cyclohexane were chosen as solvents for PMMA and PS, respectively. A 5/95 v/v % mixture of carbon tetrachloride and cyclohexane was used to improve the interlayer adhesion.[14] A portion of 10 g/L of PMMA and PS solutions was prepared using a magnetic heater stirrer. To fully homogenize, all solutions were sonicated for two 15-min periods. Sonication was used as a two-step process to avoid any solvent boiling and polymer degradation. Also, a 25 g/L PMMA solution was prepared to be cast as mechanical supporting substrate.

The machine operated at 3000 rpm for 2 h. Afterward, the chamber was detached from the machine and kept in a vacuum oven at 35 and 45°C for a 3-h rest in each step to eliminate solvent residue. In the second step, an appropriate amount of dispersion was injected into the chamber. This layer had to be deposited between PMMA and PS layers. The machine operated at 2750 rpm for 3 h. After detaching the chamber, a 2-h temperature schedule at 25°C followed by overnight at 35°C was

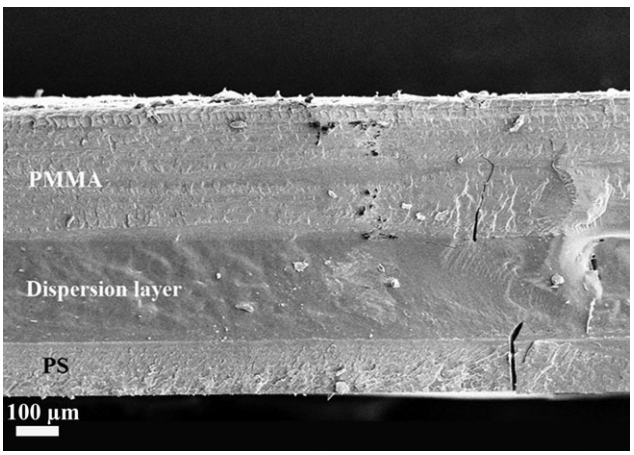

Figure 2. The SEM image of sandwiched dispersion's cross section, which approves interface formation between the layers.

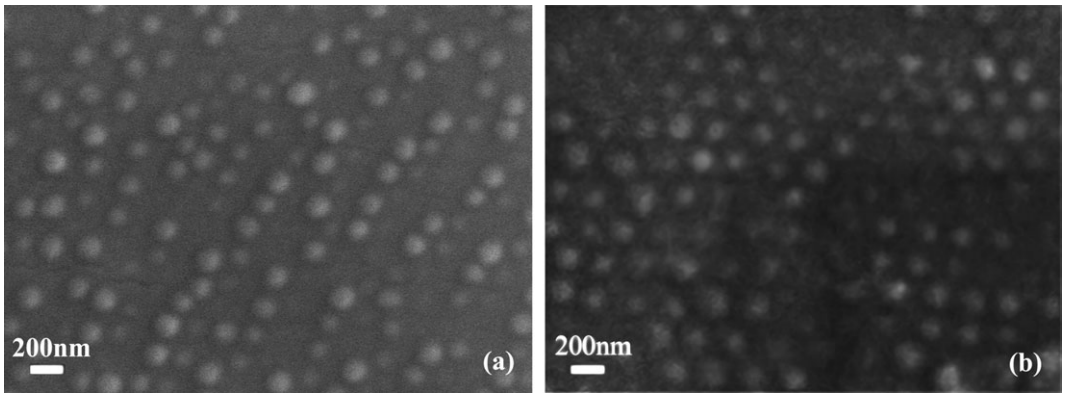

Figure 3. The SEM images of cross section of samples S1 (a) and S2 (b).

employed. In the next step, an appropriate volume of the PS solution was injected into the chamber and operated for 2 h at 2750 rpm. The chamber was isolated from the machine and dried in a vacuum oven at 35 and 45°C with a 2-h rest after each step. Finally, the process was repeated for a 10 g/L PMMA solution under the same conditions. This sample was coded as S3. The samples' code and description are compiled in Table I. The sample S1 contains one layer of dispersion, which was prepared using a ZEHNTNER-ZUA 2000 film applicator (Sissach, Switzerland). The sample S2 is composed of a PMMA layer, as supportive layer, and a dispersion layer were cast via spin-casting technique.

Characterization

The microstructure of samples was characterized via scanning electron microscopy (scanning electron microscopy (SEM), LEO model 1455VP, Cambridge, England). The reflectance and transmittance curves of samples were obtained by a Color-Eye 7000 A spectrophotometer (Grand Rapids, The USA). In addition, CIE $L^*a^*b^*c^*h$ values of these curves were calculated at 10° standard observer and under D65 illuminant. The effects of observer's viewing angles on color were considered using a CE 741 GL goniospectrophotometer (Grand Rapids, The USA) with incident beam at a fixed angle (45°) and reflected beam at 20, 45, 75, and 110° aspecular angles.

RESULTS AND DISCUSSION

Interface Formation Between the Layers

In solvent casting of polymers, the most important issue is to find an appropriate solvent system for the interface to be generated, that is, a solvent for the polymer in its own layer and an anti-solvent for the polymer in the layer beneath it. To put it simply, the solvents do not cross-solve the two polymers during a bilayer deposition. As mentioned before, acetone was used as solvent for PMMA and a mixture of cyclohexane and carbon tetrachloride as solvent for PS.[14] Apart from these two layers, the middle layer of the system is a waterborne one. Thus, the solvent of this layer, water, could not dissolve the PMMA layer. Figure 2 shows the SEM image of the sandwiched dispersion's cross section. As it is observable in this figure, interface formation between the PMMA and dispersion layers is confirmed the appropriate solvent selection for both layers. As the PS layer is sensitive to water and would typically become opaque, it must be ensured that the dispersion layer is completely dried before the PS layer is deposited. Due to this fact that dispersion's medium is acrylate-based, cyclohexane does not have any influence on the dispersion layer. Figure 2 approves this claim and the formation of sharp interface between dispersion and PS layers is clearly observed.

Effects of Centrifugal Force on Rearrangement of Particles in Dispersion Phase

The spin-casting machine operates on the basis of centrifugal forces. This type of force naturally affects the arrangement of particles. The SEM images of samples S1 and S2 vividly show a pattern resulted from this effect (Figure 3). In case of sample S1, the particles have no specific arrangements and are self-assembled [Figure 3(a)]; however in sample S2, hexagonal structures are distinguishable [Figure 3(b)], which result from centrifugal forces. Indeed, achieving long-range orders and defect-free periodic structures requires additional measures such as applying shear forces.[30–32] This approach provides long-range positional and orientational order that is taking the advantages of centrifugal forces. In the case of sample S1 that is prepared by self-assembly approach, which is simple and cost effective, irregular defects such as dislocation and missing particles restrict the size of defect-free photonic structure. Therefore, the lattice symmetry in sample S1 resulting from self-assembly is limited. The centrifugal forces and corresponding stresses, which are the basis of spin-casting approach, cause defects to decrease

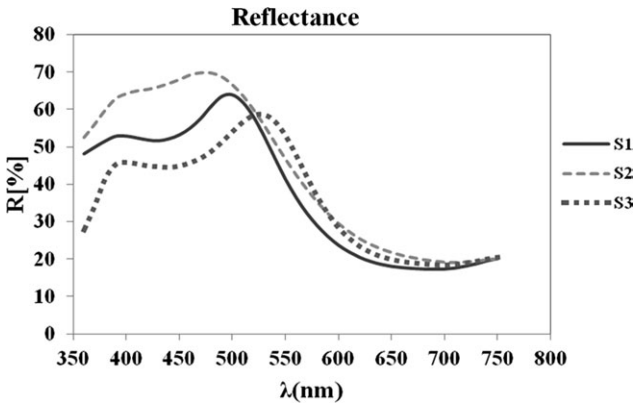

Figure 4. The reflectance curves of samples S1, S2, and S3.

Table II. The CIE $L^*a^*b^*c^*h$ Values under 10°/D65 Standard Conditions of the Reflectance Curves and Visually Observed Color of the Samples

Sample	L^*	a^*	b^*	c^*	h°	Observed color
S1	68.18	−26.6	−14.5	30.2	208	Bluish green
S2	72.5	−16.9	−22.3	27.9	232	Turquoise
S3	73.8	−28.8	−2.5	28.9	184	Green

Table III. The CIE $L^*a^*b^*c^*h$ Values under 10°/D65 Standard Conditions of the Transmittance Curves and Visually Observed Color of the Samples

Sample	L^*	a^*	b^*	c^*	h°	Observed color
S1	58.1	21.4	7.8	22.7	20.1	Scarlet
S2	64.2	13.7	28.8	31.9	64	Orange
S3	78	18.2	7.1	19.5	21	Scarlet

in sample S2 and provide an efficient way of fabricating large-scale PC. In fact, these forces make the short-range orders of particles convert to long-range orders.

Such arrangements could also change the interparticle distances, which could in turn change the color of the reflected beam (eq. 1). This could justify the change in the reflected wavelengths between samples S1 and S2. The dispersion particles are 160 nm in size, therefore spacing voids (d) for a hexagonal structure would be 130.64 nm. As the effective refractive index of the samples is 1.56, to have a maximum wavelength (λ_{max}) the angle of incidence in eq. (1) must be 0°. Hence, the calculated value for λ_{max} is 410 nm, which corresponds to a blue color.

Optical Properties of the Sandwiched Dispersion

Figure 4 shows the reflectance curves, which were obtained using a spectrophotometer. In addition, the CIE $L^*a^*b^*c^*h$ values together with visually observed color of samples S1, S2, and S3 are listed in Table II.

As it is obvious in Figure 4 and Table II, the color of sample S2, prepared by a spin-casting machine is turquoise. This is in good agreement with its calculated value using equation 1. The color of sample S1 which lack a specific arrangement on the other hand is observed to be bluish green and further exemplified by its CIE $L^*a^*b^*c^*h$ values.[29] Sample S3 includes the sandwiched dispersion layer between PS and PMMA layers. Although these polymeric layers are transparent, based on Snell's law, these layers are able to affect the optical properties of dispersion layer. Sample S3 have a green shift as compared to sample S2.

The transmittance curves of samples are shown in Figure 5. The CIE $L^*a^*b^*c^*h$ values calculated from measured transmittance curves of the three samples together with their visually observed colors are listed in Table III. In fact, comparing data in Tables II and III shows that transmittance curves are complementary to the corresponding reflectance curves due to a change in viewing geometry.

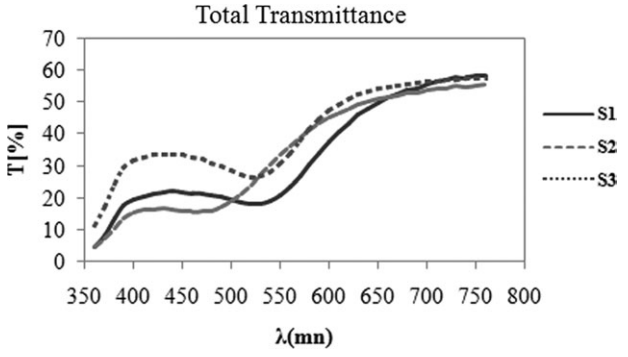

Figure 5. The transmittance curve of samples S1, S2, and S3.

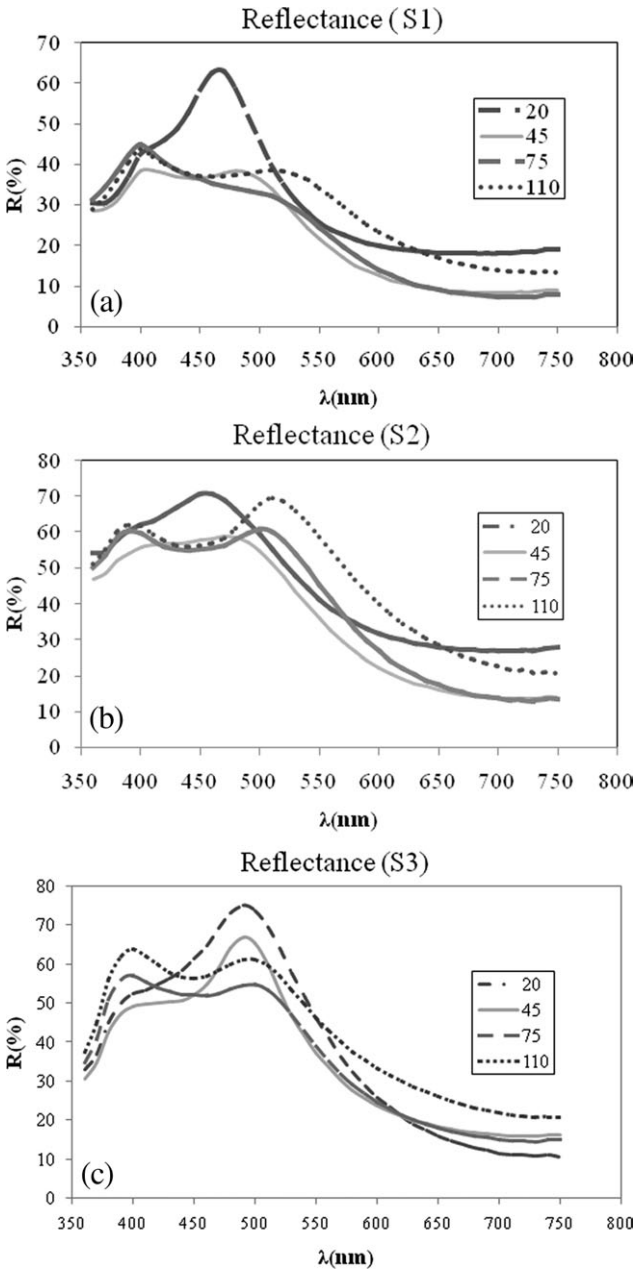

Figure 6. The goniospectrophotometeric curves of samples (a) S1, (b) S2, and (c) S3.

Table IV. The Colorimetric Data at Four Angles of Observation under 10°/D65 Standard Conditions and Visually Observed Color for Samples S1, S2, and S3

Sample	Angle	L^*	a^*	b^*	c^*	h°	Observed color
S1	20°	61.5	−30.5	−6.85	31.2	257.4	Greenish blue
	45°	54.7	−21.6	−16.6	27.2	232.5	Turquoise
	75°	55.7	−19.2	−14.3	23.9	233.3	Turquoise
	110°	63.1	−8.1	−13.6	15.7	210.8	Bluish green
S2	20°	72.0	−24.1	−8.2	25.4	251	Greenish blue
	45°	67.2	−22.8	−16.6	28.2	232	Turquoise
	75°	71.0	−13.5	−22.6	26.3	210	Bluish green
	110°	78.9	−3.1	−20.8	21.1	188.5	Green
S3	20°	79.9	−14.5	−24.9	28.8	220	Bluish green
	45°	77.8	−8.6	−17.6	19.5	216.3	Bluish green
	75°	78.0	−8.7	−10.5	13.6	210.5	Bluish green
	110°	81.4	−5.5	−9.1	10.6	206	Bluish green

A goniospectrophotometric technique was used to show the variations in the reflectance curves of samples S1, S2, and S3 with changes in the angle of observation. Such variations are depicted in Figures 6(a–c), respectively. The reflectance curves of sample S1 [Figure 6(a)] show a sudden drop of a pronounced blue peak at approximately 450 nm for the 20° aspecular angle and a gradual appearance of a shifted peak to longer wavelengths as the angle of observation is increased, becoming 525 nm for the 110° aspecular angle. The same behavior is seen for the reflectance curve of sample S2 as illustrated in Figure 6(b). Figure 6(c) shows a similar behavior but to a much lower extent for sample S3. To show the final effect of increased angle of observation on color variations (i.e., opalescence), the reflectance curves were converted to colorimetric data using the 1964 CIE standard observer and D65 standard illuminant. Such data in addition to visually observed color equivalences for samples S1, S2, and S3 are collectively illustrated in Table IV. This table confirms the conclusions reached from the spectrophotometric curves. For example, increasing the angle of observation changes the hue angle from 257.4 to 210.8 for sample S1; 251 to 188.5 for sample S2; and 220 to 206 for sample S3 as is depicted in Figure 7. This is in complete agreement with the visually observed hues illustrating a green shift to various extents for such samples.

As mentioned earlier, color of reflected light from PC depends on the angle of observation. By sandwiching a dispersed sample between two polymeric layers this property tends to diminish (see Table IV). Figure 7 showing changes in hue angle with variations in the aspecular angle confirms that such variations are much more limited for sample S3 which is also confirmed visually.

Figure 8 demonstrates a schematic diagram of a sandwiched sample. When light reaches the polymeric dispersion beads after refraction through the other clear polymers, two light pathways become possible. A part of light could pass through the bulk of the sandwiched sample with minimal variation in direction (pathway 1). Another part of light could reflect from beads

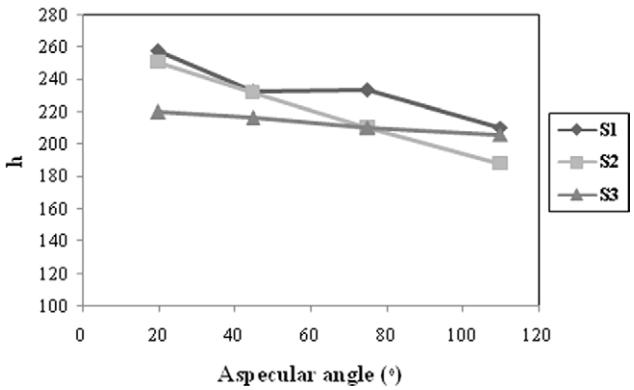

Figure 7. The effect of angular changing on the hue angle.

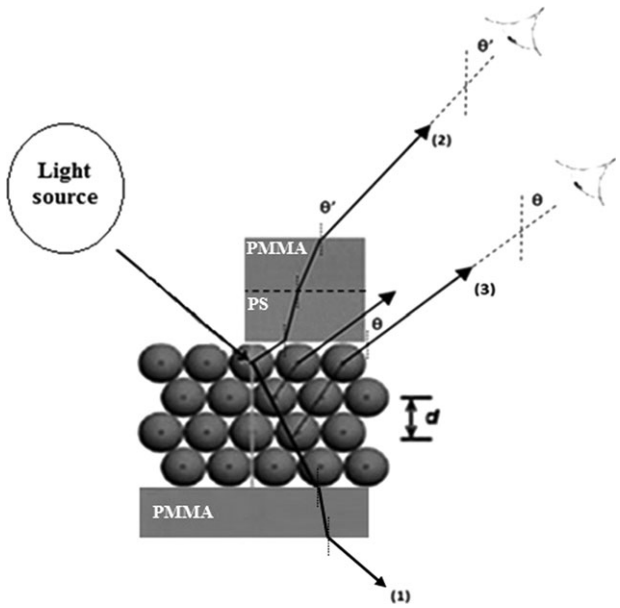

Figure 8. The schematic diagram of refractive mechanism.

(pathway 2) and also refract at each polymer interface due to differences in the refractive indices. These refractions cause the ray 2 enters to medium with a different pathway compared to that of ray 3 (in sample S2). Such structure cause color divisions, which means that the transmitted light through the bulk (i.e., pathway 1) could be complementary to the refracted rays.

The range of visible wavelengths escaping from a dispersion layer could decrease due to the critical angle when the light passes through air then a successive layers of transparent, dispersed, and again transparent polymeric layers of different refractive indices and finally through air. For a completely well-dispersed system, the refracted light would be complementary to the transmitted. This is approximately reached for sample S3. This brings to mind the idea of using sample S3 as an interference filter.

CONCLUSION

A spin-casting machine was designed and used to study the effect of centrifugal force on the arrangement of styrene-based nanoparticles. The formation of interface between layers was approved by SEM technique, which shows an appropriate solvent selection. In addition, the SEM images of prepared samples' cross sections indicate that nanoparticles arrange themselves in a near to beehive hexagonal structures. This could partly be attributable to centrifugal forces. Such arrangements tend to change the resultant color of a sample. Influence of particle arrangements on color changes at various angles of viewing and observation was studied using a goniospectrophotometer. The dispersion of styrene-based nanoparticles restricts some reflecting wavelengths due to changes in the refractive indices of the sandwiched samples.

REFERENCES

1. Paquet, C.; Kumacheva, E. *Nano Mater. Today.* **2008,** *111*, 48.
2. Stoeffler, K.; Dubois, C.; Ajji, A.; Guo, N.; Boismenu, F.; Skorobogatiy, M. *Polym. Eng. Sci.* **2010,** *50*, 1122.
3. Lange, B.; Fleischhaker, F.; Zentel, R. *Macromol. Rapid Commun.* **2007,** *28*, 1291.
4. Edrington, A. C.; Urbas, A. M.; DeRege, P.; Chen, C. X.; Swager, T. M.; Hadjichristidis, N.; Xenidou, M.; Fetters, L. J.; Joannopoulos, J. D.; Fink, Y.; Thomas, E. L. *Adv. Mater.* **2001,** *13*, 421.
5. Skorobogatiy, M.; Yang, J. Fundamentals of Photonic Crystal Guiding; Cambridge University Press: New York, **2009;** pp 1–13.
6. Skorobogatiy, M.; Guo, N. *Opt. Lett.* **2007,** *32*, 900.
7. Large, M. C. J.; Poladian, L.; Barton, G. W.; Eijkelenborg, M. A. Microstructured Polymer Optical Fibres; Springer: New York, **2007;** pp 21–38.
8. Tilley, R. Colour and Optical Properties of Material; Wiley: Chichester, **1999.**
9. Ruhl, T.; Spahn, P.; Winkler, H.; Hellmann, G. P. *Progr. Colloid Polym. Sci.* **2004,** *129*, 82.
10. Ruhl, T.; Spahn, P.; Hellmann, G. P. *Polymer* **2003,** *44*, 7625.
11. Ruhl, T.; Hellmann, G. P. *Macromol. Chem. Phys.* **2001,** *202*, 3502.
12. Ruhl, T.; Spahn, P.; Winkler, H.; Hellmann, G. P. *Macromol. Chem. Phys.* **2004,** *205*, 1385.
13. Lange, B.; Metz, N.; Tahir, M.; Theato, P.; Fleischhaker, F.; Schroder, H.; Muller, W.; Tremel, W.; Zentel, R. *Macromol. Rapid Commun.* **2007,** *28*, 1987.
14. Gao, Y.; Guo, N.; Gauvreeau, B.; Rajabian, M.; Skorobogata, O.; Pone, E.; Zaberda, O.; Martinu, L.; Dubois, C.; Skorobogatiy, M. *J. Mater. Res.* **2006,** *21*, 2246.
15. Lange, B.; Fleischhaker, F.; Zentel, R. *Phys. Status Solidi A* **2007,** *204*, 3618.
16. Egen, M.; Zentel, R. *Macromol. Chem. Phys.* **2004,** *205*, 1479.
17. Egen, M.; Braun, L.; Zentel, R.; Tannert, K.; Frese, P.; Reis, O.; Wulf, M. *Macromol. Master Eng.* **2004,** *289*, 158.
18. Egen, M.; Voss, R.; Griesebook, B.; Zentel, R. *Chem. Mater.* **2003,** *15*, 3786.
19. Kazmierczak, T.; Song, H.; Hiltner, A.; Baer, E. *Macromol. Rapid Commun.* **2007,** *28*, 2210.
20. Spahn, P.; Finlayson, C. E.; Etah, W. M.; Snoswell, D. R. E.; Baumberg, J. J.; Hellmann, G. P. *J. Mater. Chem.* **2011,** *21*, 8893.
21. Finlayson, C. E.; Spahn, P.; Snoswell, D. R. E.; Yates, G.; Kontogeorgos, A.; Haines, A. I.; Hellmann, G. P.; Baumberg, J. J. *Adv. Mater.* **2011,** *23*, 1540.
22. Gauvreau, B.; Geo, N.; Schicker, K.; Stoeffler, K.; Boismenu, F.; Ajji, A.; Wingfield, R.; Dubois, C.; Skorobogatiy, M. *Opt. Express.* **2008,** *16*, 15677.
23. Kim, S. H.; Lee, S. Y.; Yang, S. M.; Yi, G. R. *NPG Asia Mater.* **2011,** *3*, 25.
24. Thelen, A. U. S. Pat. 3,914,023, (**1975).**
25. Shaghaghi, M. M.Sc Dissertation, Institute for Color Science and Technology, October **2010.**
26. Finlayson, C. E.; Haines, A. I.; Snoswell, D. R. E.; Kontogeorgos, A.; Vignolini, S.; Baumberg, J. J.; Spahn, P.; Hellmann, G. P. *Appl. Phys. Lett.* **2011,** *99*, 261913-1-4.
27. Shamshiri, M. R. M.Sc Dissertation, Institute for Color Science and Technology, November **2010.**
28. Shamshiri, M. R.; Yousefi, A. A.; Ameri, F.; Shamshiri, M. R.; Yousefi, A. A.; Ameri, F. In: Proceedings of 11th International Conference on Frontiers of Polymers and Advanced Materials; South Africa, **2011.**
29. Shamshiri, M. R.; Yousefi, A. A.; Ameri, F. *J. Color Sci. Technol.* **2011,** *5*, 69.
30. O'Neill, M.; Kelly, S. M. *Adv. Mater.* **2011,** *23*, 566.
31. South, A. B.; Whitmire, R. E.; Garcia, A. J.; Lyon, L. A. *Appl. Mater. Interfaces.* **2009,** *1*, 2747.
32. Angelescu, D. B.; Waller, J. D.; Adamson, D. H.; Deshpande, P.; Chou, S. Y.; Register, A.; Chaikin, P. M. *Adv. Mater.* **2004,** *16*, 1736.